# SUPPLEMENTARY MATERIAL 2 TO:

Tramm, F., Rzepa, G., Budzyń, B., Kozub-Budzyń, G. A., Dybaś, J. & Sláma, J., 2024. Raman microspectroscopy of monazite-(Ce) and xenotime-(Y): examples from experiments and nature. *Annales Societatis Geologorum Poloniae*, 94: 297–328.

## COMPOSITIONAL AND TEXTURAL DESCRIPTION OF INVESTIGATED MONAZITE-(Ce) AND XENOTIME-(Y) FROM EXPERIMENTAL PRODUCTS

Raman microspectroscopy, EPMA and LA-ICPMS measurements on monazite-(Ce) and xenotime-(Y) grains from products of experiments, (Exp1: 200 MPa / 350 °C, Exp2: 400 MPa / 450 °C, Exp3: 600 MPa / 550 °C, Exp4: 800 MPa / 650 °C, Exp5: 1000 MPa / 750 °C) were placed close to each other (Fig. S1). The experiments were conducted in previous works (Budzyń and Kozub-Budzyń, 2015; Budzyń *et al.*, 2015, 2017). Monazite-(Ce) grains from Exp1 display dissolution pits and microporosity resulting from fluid-mediated coupled dissolution-reprecipitation reactions (Fig. S1A–C). Patchy zoning, another typical result of coupled dissolution-reprecipitation processes, was not documented most likely due to a low current used during BSE imaging to prevent sample damage. Monazite-(Ce) grains from Exp2 show cracks and microporosity, which are partially filled with secondary REE-rich steacyite representing the dominant secondary product of experiments at these *P-T* conditions (400 MPa / 450 °C; Fig. S1D–G). Numerous grains of REE-rich steacyite also formed at the rim of the monazite-(Ce) grains, which are occasionally accompanied by fine grains of secondary fluorcalciobritholite (Fig. S1F). In products of Exp3, monazite-(Ce) grains display alteration textures with fine crystals of fluorcalciobritholite representing the dominant secondary phase (Fig. S1I–M). One monazite-(Ce) grain displays patchy zoning even at a low current (Fig. S1I, L). The unaltered domains of monazite-(Ce) from Exp1–Exp3 are compositionally similar to that of Burnet monazite-(Ce), whereas altered domains are depleted in Th, U and Pb (Supplementary Table B3).

Grains from Exp4 (800 MPa / 650 °C) show microporosity at the rim, which are partially filled by secondary fluorcalciobritholite (Fig. S1N–O). Occasionally, cheralite [$CaTh(PO_4)_2$] forms fine aggregates together with the fluorcalciobritholite near the phase boundary of monazite-(Ce) (Fig. S1P). Monazite-(Ce) grains from Exp5 are commonly overgrown by several-micron-sized fluorcalciobritholite grains (Fig. S1R–V). A shard of residual glass, in which several monazite-(Ce) grains are embedded represents an exception (Fig. S1W–X). The monazite-(Ce) grains occasionally display porosity at their rims, and small crystals of fluorcalciobritholite formed between grains. The monazite-(Ce) grains from Exp4 and Exp5 display a similar composition to that of Burnet monazite-(Ce) (Supplementary Table B3).

Chondrite-normalized data of unaltered monazite-(Ce) domains from Exp1–Exp3 show similar patterns to that of Burnet monazite-(Ce), which display typical LREE >> HREE shape including a slight increase from La to Ce, a decreasing slope from Sm to Lu, and negative anomalies of Eu and Y (Fig. S2A–D). Altered domains demonstrate significant depletion of the HREE (Fig. 2B–D). Chondrite-normalized data show similar patterns to those of the Burnet monazite-(Ce) (Fig. S2E, F), except occasionally less pronounced negative anomalies of Eu and Y. The latter may suggest the incorporation of Eu released from micas during partial melting in the experiments via fluid-induced coupled dissolution-reprecipitation processes at the submicron scale (cf., Budzyń *et al.*, 2021).

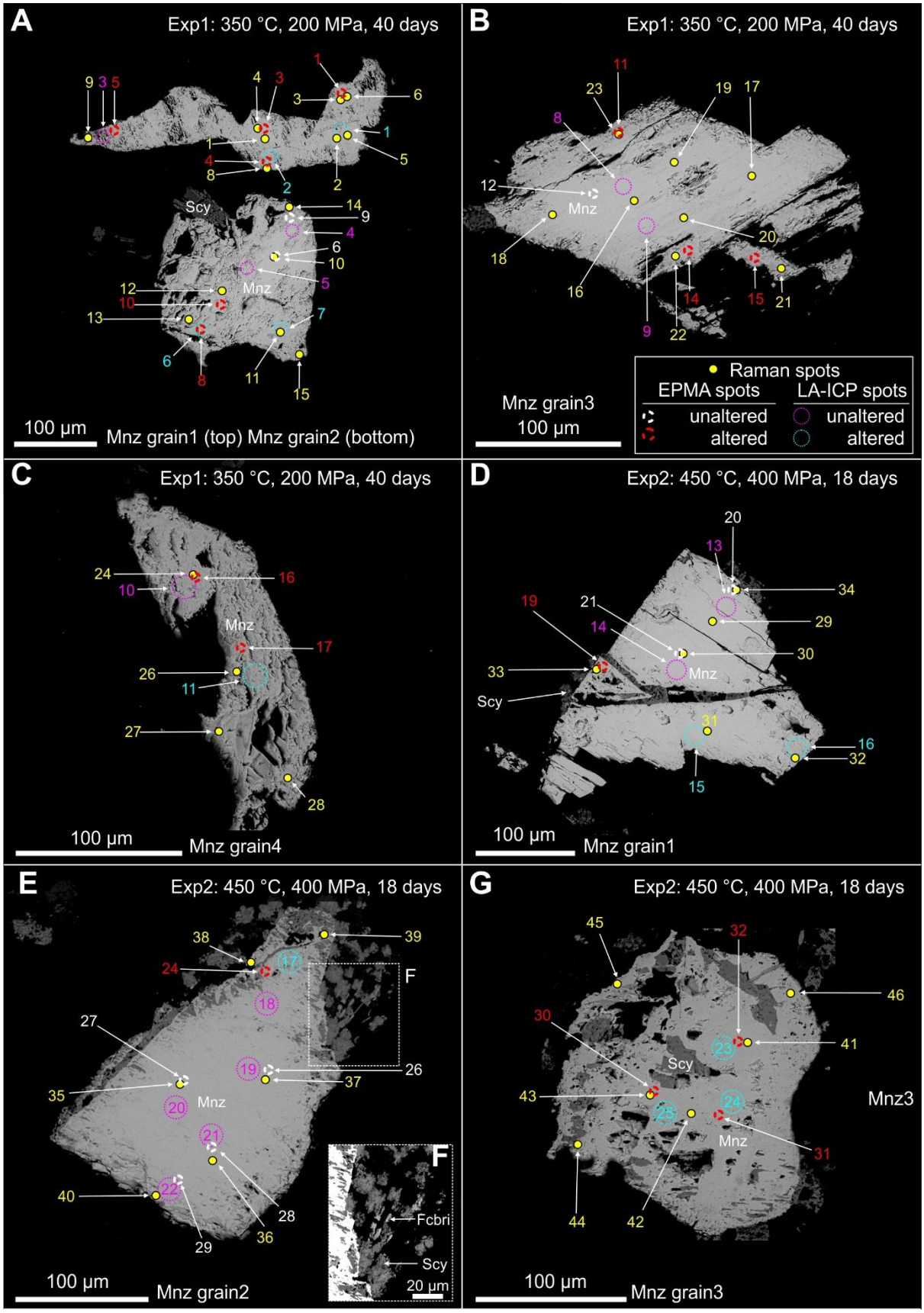


**Fig. S1.** BSE images of investigated monazite-(Ce) grains from Exp1–Exp5 with Raman, EPMA and LA-ICPMS analytical spots. Mineral abbreviations: Cher – cheralite, Mnz – monazite-(Ce), Scy – steacyite, Fcbri – fluorcalciobritholite.

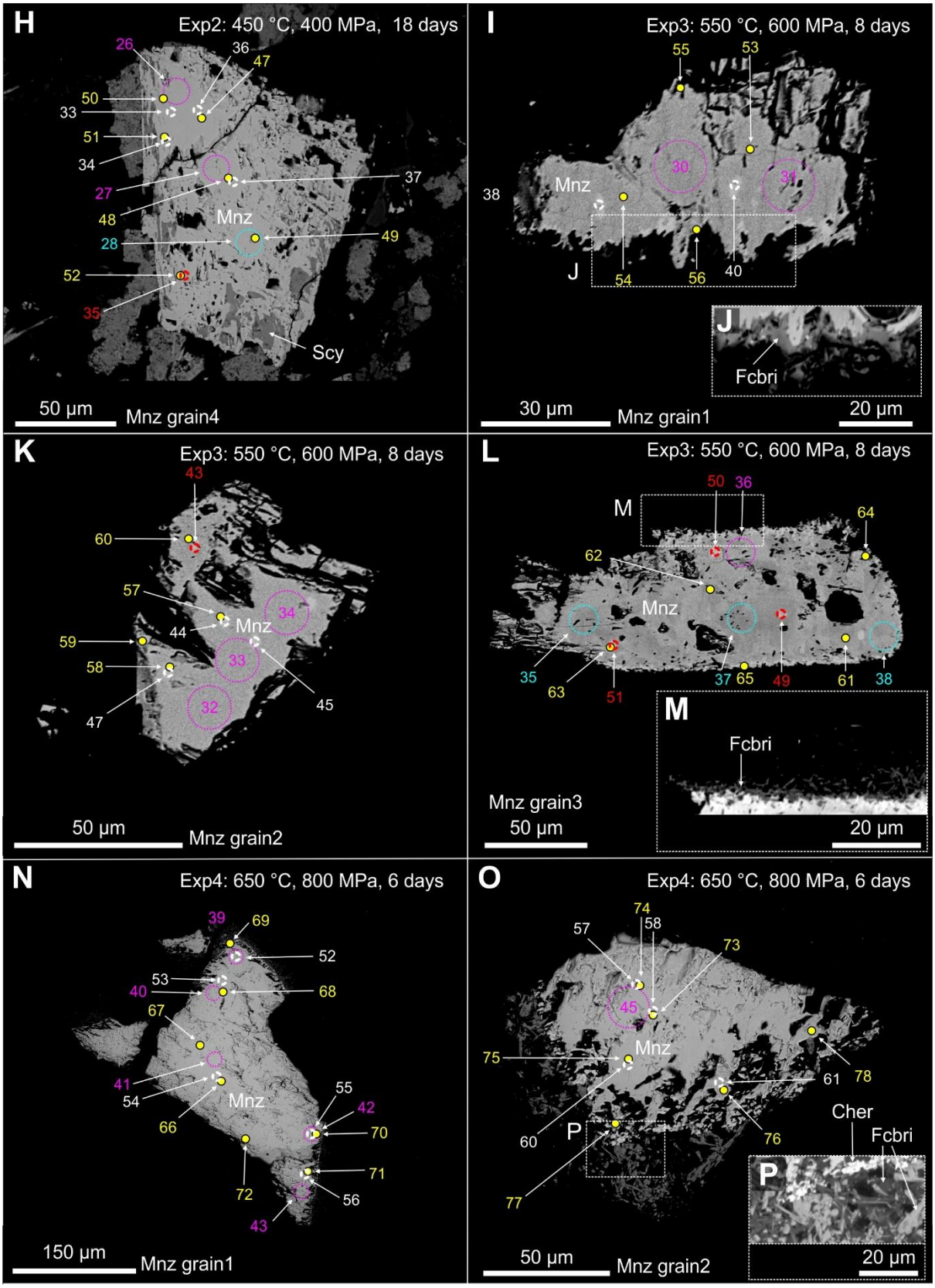


**Fig. S1.** Continued.

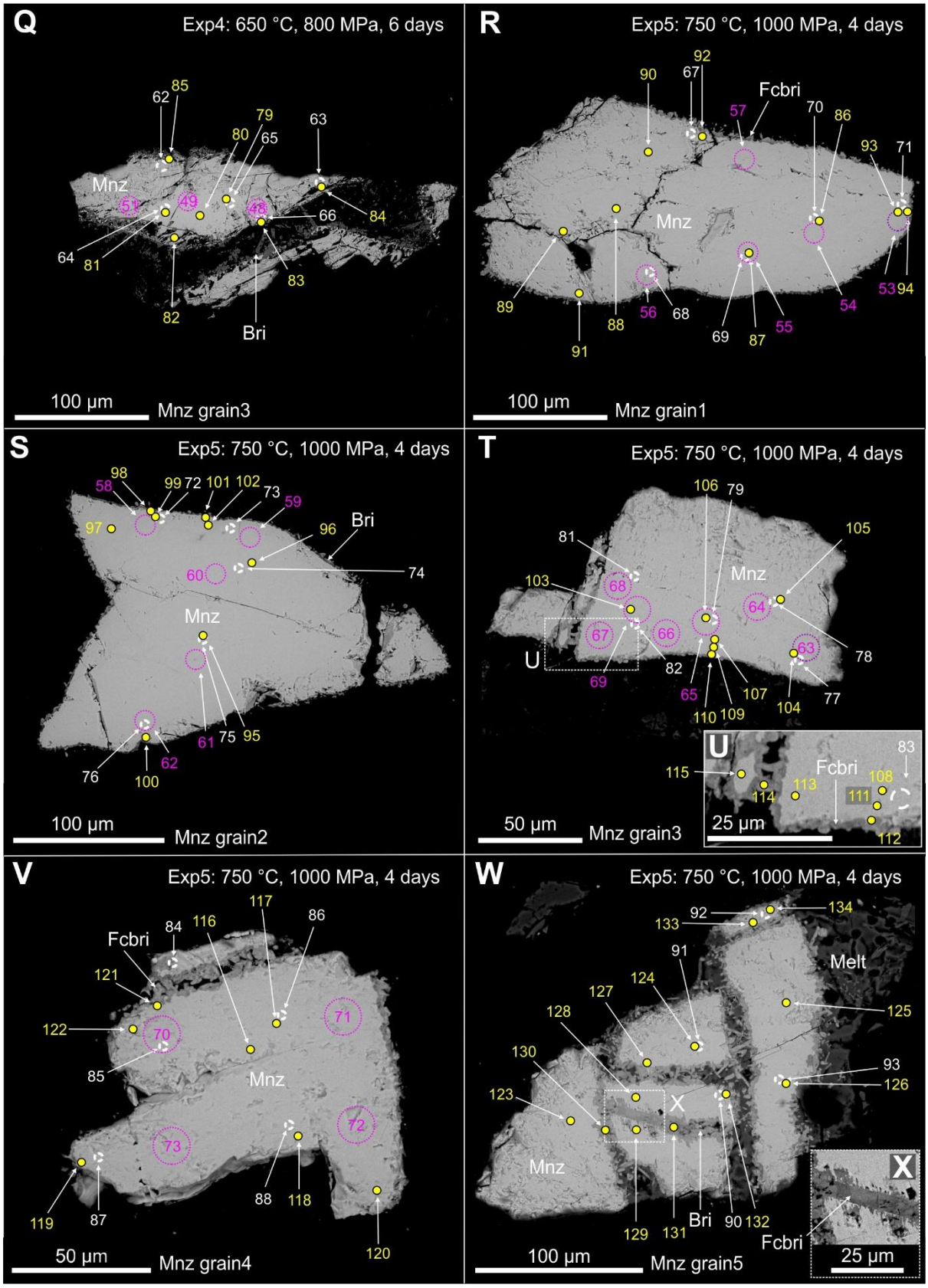


**Fig. S1.** Continued.

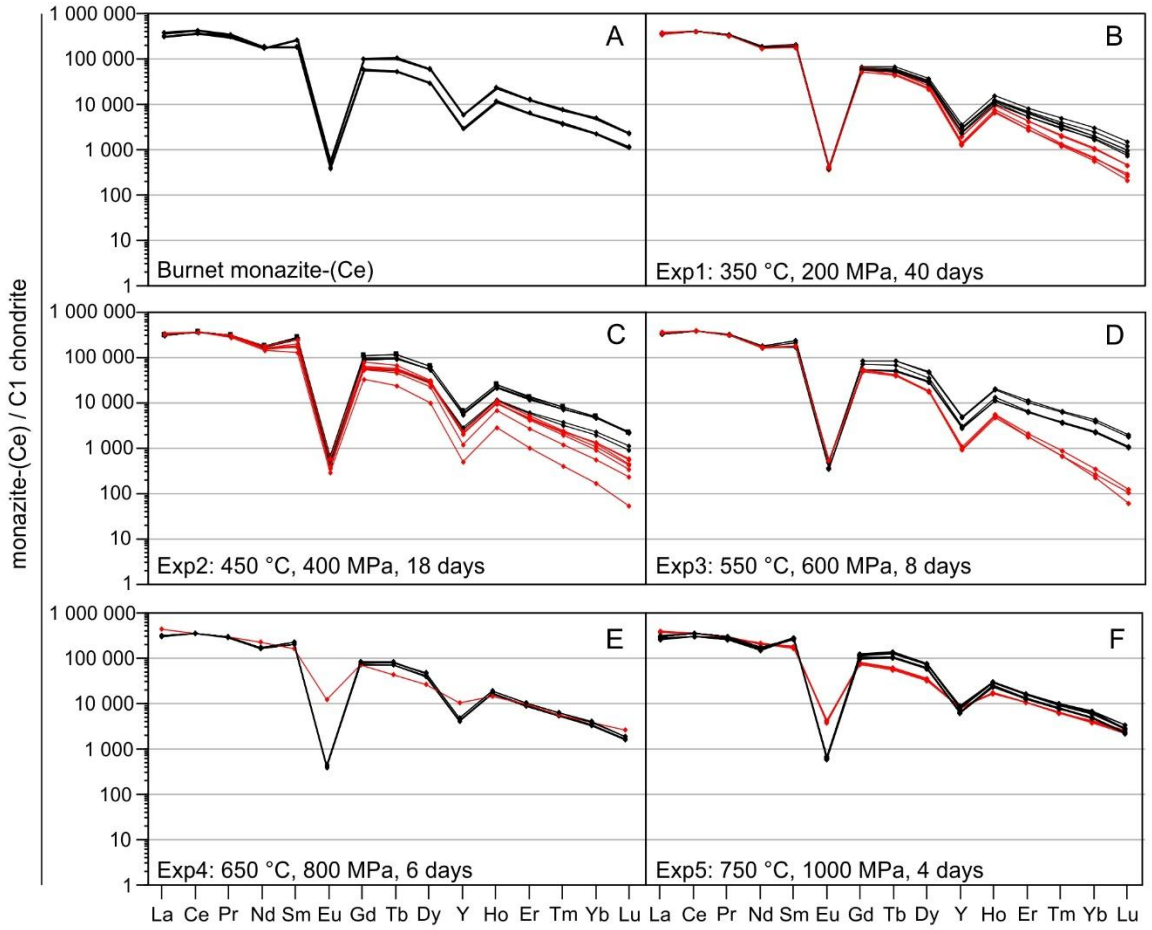


**Fig. S2.** Chondrite-normalized REE distribution patterns of Burnet monazite-(Ce) and monazite-(Ce) from experimental products. Composition of C1 chondrite after McDonough and Sun (1995). Black line – unaltered monazite-(Ce), red line – altered monazite-(Ce).

Xenotime-(Y) grains from the products of experiments at low *P-T* conditions (Exp1–Exp3) are homogeneous in BSE images and lack textural evidence of fluid-mediated alteration (Fig. S3A–H). First textural signs of fluid-mediated alteration of xenotime-(Y) are shown in grains from Exp4–Exp5, which display dissolution pits, overgrowth and partial replacement of Y-rich fluorcalciobritholite (Fig. S3I–L).

Chondrite normalized patterns of xenotime-(Y) from Exp1 and Exp2 (200 MPa / 350 °C and 400 MPa / 450 °C) show similarities to NWFP xenotime-(Y), which follows LREE << HREE patterns typical for xenotime-(Y), and demonstrate a steep increasing slope from La to Tb (Fig. S4A–C). These include variations from La to Nd and small variations from Tm to Lu in xenotime-(Y). Xenotime-(Y) grains from Exp3–Exp5 (600 MPa / 550 °C, 800 MPa / 650 °C, 1000 MPa / 750 °C) show homogenous REE distribution from La to Lu (Fig. S4D–F).

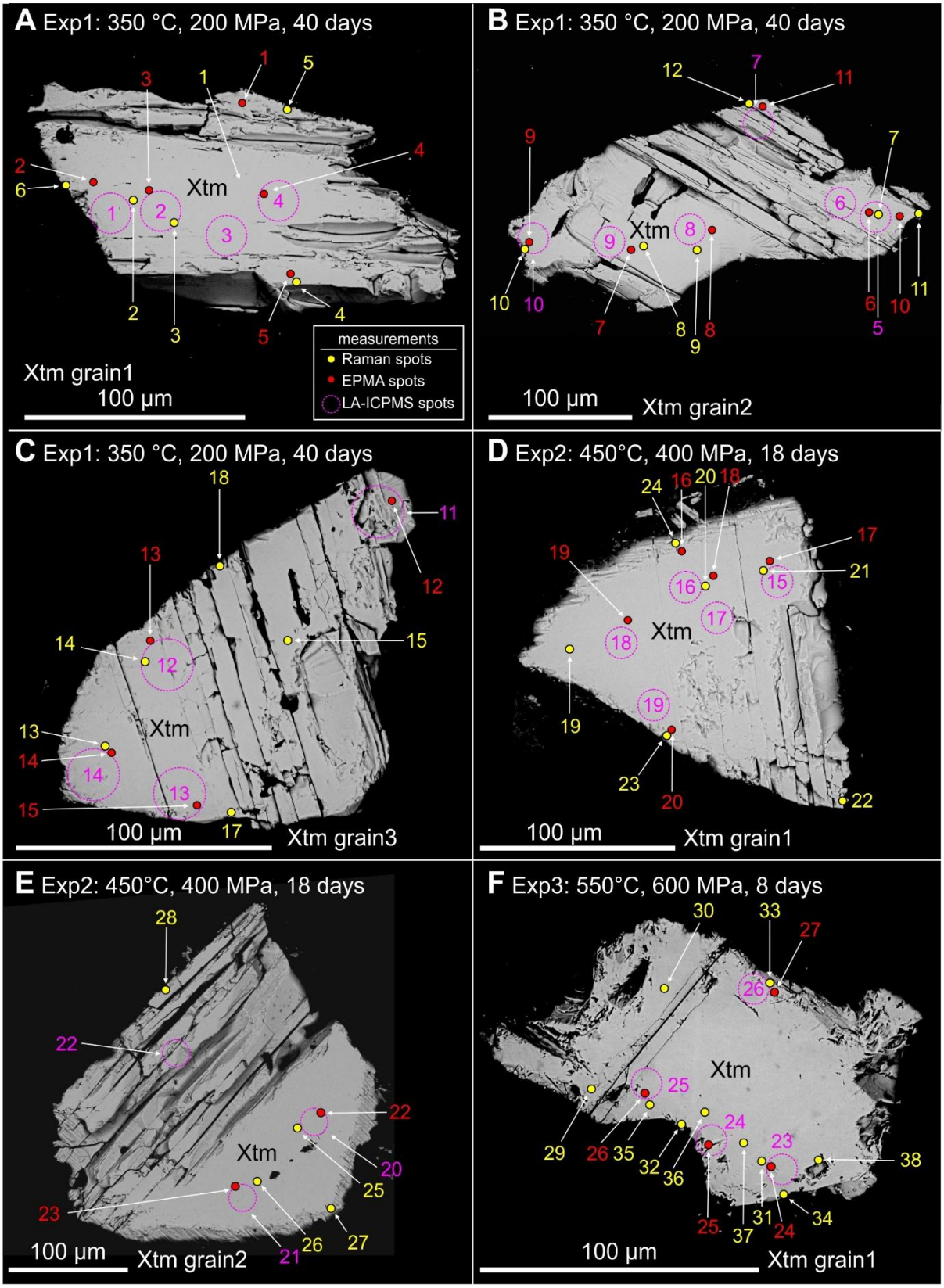


**Fig. S3.** BSE images of investigated xenotime-(Y) grains from Exp1–Exp5 with Raman, EPMA and LA-ICPMS analytical spots. Mineral abbreviations: YFcbri – Y-rich fluorcalciobritholite, Xtm – xenotime-(Y).

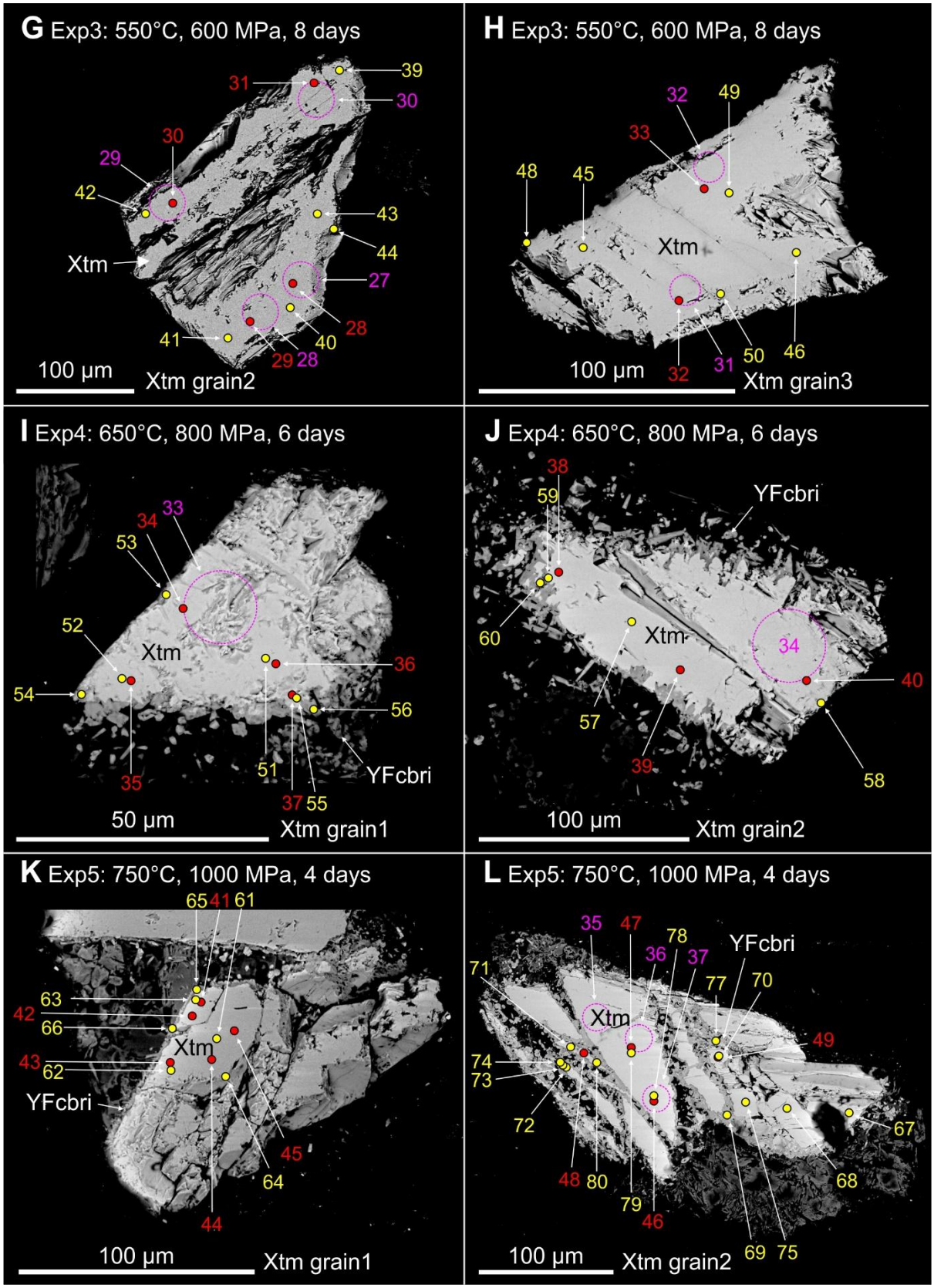


**Fig. S3.** Continued.

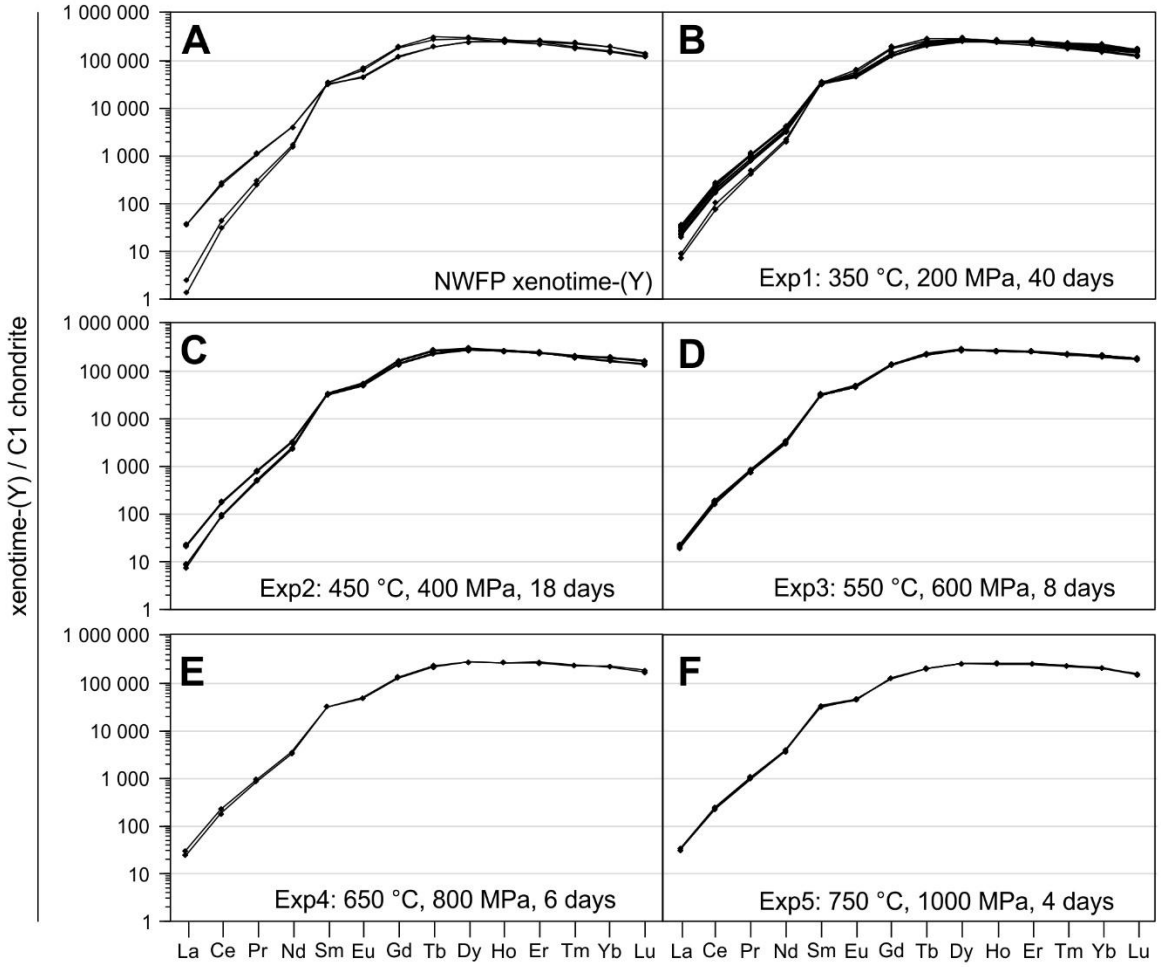


**Fig. S4.** Chondrite-normalized REE patterns of NWFP xenotime-(Y) and xenotime-(Y) from experimental products. C1 chondrite composition from McDonough and Sun (1995).

**Raman spectra of monazite-(Ce) and xenotime-(Y) collected with the 780 nm laser**

A monazite-(Ce) spectrum from Exp1 collected with instrument A (Thermo Scientific DXR Raman Microscope, see methodology in the corresponding article for details) with a 780 nm laser displays extensive luminescence effects, which superimpose the primary Raman features (Fig. S5). Luminescence effects are present in a very similar shape in reference spectra of $LaPO_4$, $CePO_4$ and $GdPO_4$ (Fig. S5B). These effects are most likely due to trace concentrations of $Nd^{3+}$ in the reference REE phosphates which cause NIR luminescence emissions related to the $^4F_{3/2} \rightarrow {}^4I_{9/2}$ transition (see fig. 3 in Lentz *et al.*, 2015). The 780 nm laser is considered unsuited for the Raman characterization of natural monazite-(Ce) if such strong luminescence effects are present.

A xenotime-(Y) spectrum collected with instrument A (780 nm), shows strong luminescence effects at low-range (100–700 $cm^{-1}$) that superimpose lattice modes and internal bending modes and mid-range luminescence effects resembling those of $LaPO_4$, $CePO_4$ and $GdPO_4$ (Fig. S6). The low-range luminescence effects in the xenotime-(Y) spectrum are contributed by the $TmPO_4$ component ($Tm^{3+}$: $^3H_4 \rightarrow {}^3H_6$; Fig. S6B).

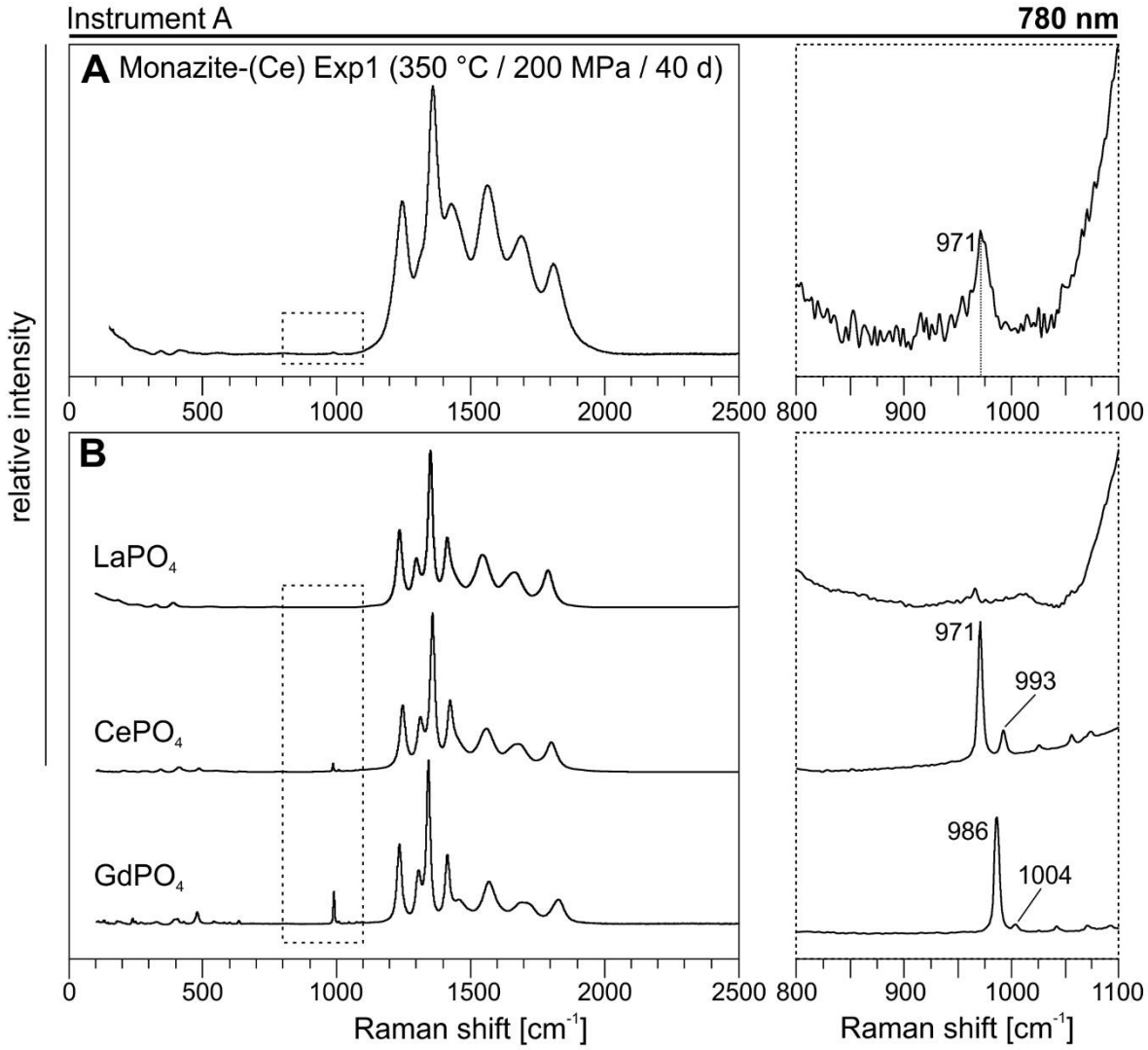


**Fig. S5.** Raman spectra (instrument A; 780 nm) of (**A**) monazite-(Ce) from Exp1 and (**B**) synthetic $LaPO_4$, $CePO_4$ and $GdPO_4$. The spectra are dominated by luminescence effects. Right side – zoomed-in spectra corresponding to dotted rectangles.

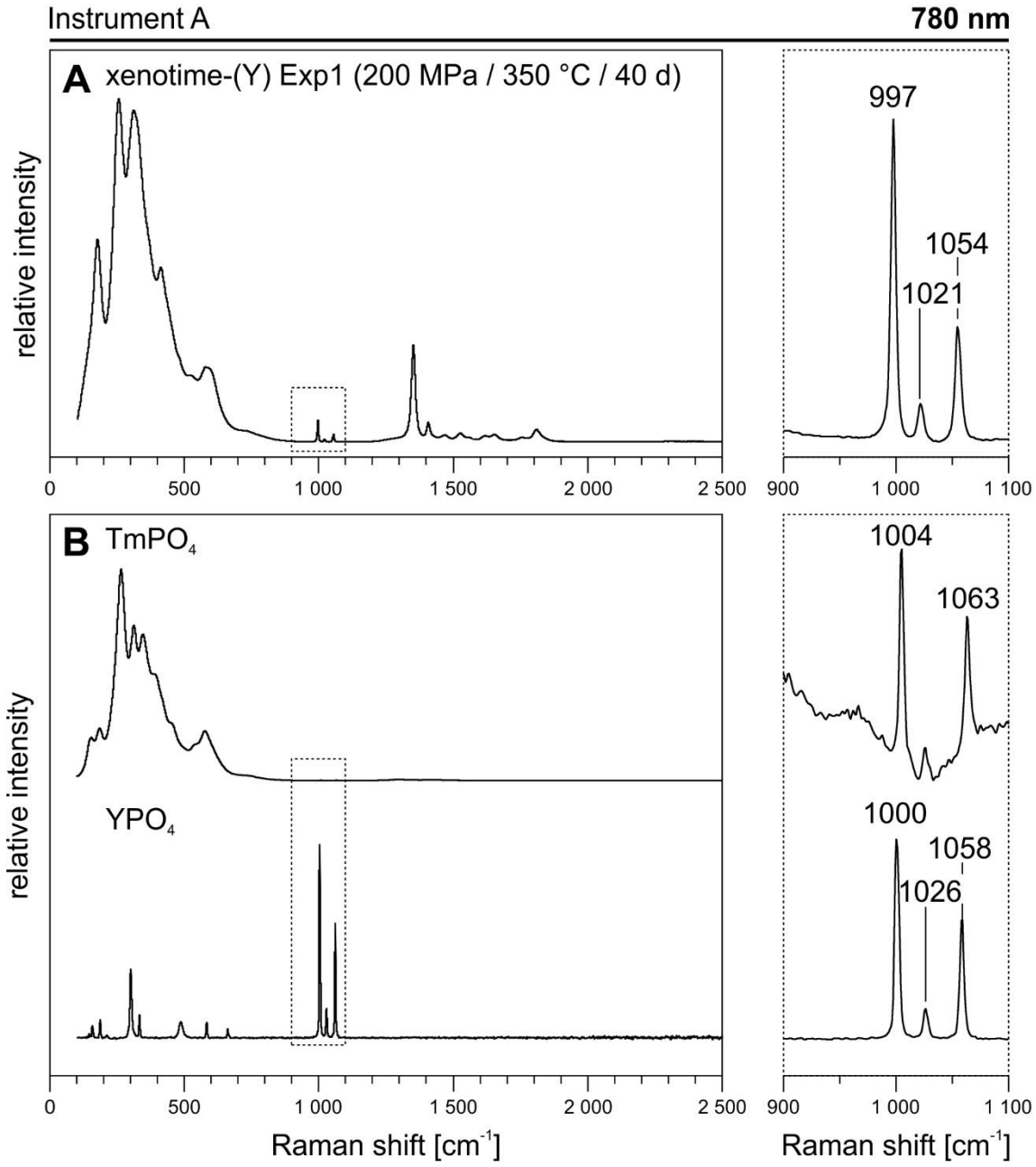


**Fig. S6.** Raman spectra (instrument A; 780 nm) of (**A**) xenotime-(Y) from Exp1 and (**B**) synthetic $TmPO_4$, and $YPO_4$. Low-range luminescence effects dominate the xenotime-(Y) and $TmPO_4$ spectra. Right side – zoomed-in spectra corresponding to dotted rectangles.

## REFERENCES

Budzyń, B. & Kozub-Budzyń, G.A., 2015. The stability of xenotime in high Ca and Ca-Na systems, under experimental conditions of 250–350°C and 200–400 MPa: the implications for fluid-mediated low-temperature processes in granitic rocks. *Geological Quarterly*, 59: 316–324.

Budzyń, B., Konečný, P. & Kozub-Budzyń, G.A., 2015. Stability of monazite and disturbance of the Th-U-Pb system under experimental conditions of 250–350 °C and 200–400 MPa. *Annales Societatis Geologorum Poloniae*, 85: 405–424.

Budzyń, B., Harlov, D., Kozub-Budzyń, G.A. & Majka, J., 2017. Experimental constraints on the relative stabilities of the two systems monazite-(Ce) – allanite-(Ce) – fluorapatite and xenotime-(Y) – (Y,HREE)-rich epidote – (Y,HREE)-rich fluorapatite, in high Ca and Na-Ca environments under P-T conditions of 200–1000 MPa and 450–750 °C. *Mineralogy and Petrology*, 111: 183–217.

Budzyń, B., Wirth, R., Sláma, J., Birski, Ł., Tramm, F., Kozub-Budzyń, G.A., Rzepa, G. & Schreiber, A., 2021. LA-ICPMS, TEM and Raman study of radiation damage, fluid-induced alteration and disturbance of U-Pb and Th-Pb ages in experimentally metasomatised monazite. *Chemical Geology*, 583: 120464.

McDonough, W.F. & Sun, S.-s., 1995. The composition of the Earth. *Chemical Geology*, 120: 223–253.

Lenz, C., Nasdala, L., Talla, D., Hauzenberger, C., Seitz, R. & Kolitsch, U., 2015. Laser-induced $REE^{3+}$ photoluminescence of selected accessory minerals – An "advantageous artefact" in Raman spectroscopy. *Chemical Geology*, 415: 1–16.